Pharm Res (2015) 32:1615–1625
DOI 10.1007/s11095-014-1561-6

RESEARCH PAPER

Alternating Magnetic Field-Induced Hyperthermia Increases Iron Oxide Nanoparticle Cell Association/Uptake and Flux in Blood–Brain Barrier Models

Mo Dan • Younsoo Bae • Thomas A. Pittman • Robert A. Yokel

Received: 4 August 2014 / Accepted: 27 October 2014 / Published online: 7 November 2014

ABSTRACT

Purpose Superparamagnetic iron oxide nanoparticles (IONPs) are being investigated for brain cancer therapy because alternating magnetic field (AMF) activates them to produce hyperthermia. For central nervous system applications, brain entry of diagnostic and therapeutic agents is usually essential. We hypothesized that AMF-induced hyperthermia significantly increases IONP blood–brain barrier (BBB) association/uptake and flux.

Methods Cross-linked nanoassemblies loaded with IONPs (CNA-IONPs) and conventional citrate-coated IONPs (citrate-IONPs) were synthesized and characterized in house. CNA-IONP and citrate-IONP BBB cell association/uptake and flux were studied using two BBB Transwell® models (bEnd.3 and MDCKII cells) after conventional and AMF-induced hyperthermia exposure.

Results AMF-induced hyperthermia for 0.5 h did not alter CNA-IONP size but accelerated citrate-IONP agglomeration. AMF-induced hyperthermia for 0.5 h enhanced CNA-IONP and citrate-IONP BBB cell association/uptake. It also enhanced the flux of CNA-IONPs across the two *in vitro* BBB models compared to conventional hyperthermia and normothermia, in the absence of cell death. Citrate-IONP flux was not observed under these conditions. AMF-induced hyperthermia also significantly enhanced paracellular pathway flux. The mechanism appears to involve more than the increased temperature surrounding the CNA-IONPs.

Conclusions Hyperthermia induced by AMF activation of CNA-IONPs has potential to increase the BBB permeability of therapeutics for the diagnosis and therapy of various brain diseases.

KEY WORDS alternating magnetic field · blood–brain barrier permeability · cross-linked nanoassemblies · flux · superparamagnetic iron oxide nanoparticles

ABBREVIATIONS

AMF	Alternating magnetic field
BBB	Blood–brain barrier
bEnd.3	A transformed murine brain/cerebral cortex endothelial cell line
Citrate IONPs	Citrate iron oxide nanoparticles
CNA-IONPs	Cross-linked nanoassembly iron oxide nanoparticles
CNS	Central nervous system
DLS	Dynamic light scattering
IONPs	Iron oxide nanoparticles
LY	Lucifer yellow
MDCKII	Madin-Darby canine kidney II cells
P_{app}	Apparent permeability coefficient

INTRODUCTION

Brain capillary endothelial cells cooperate with pericytes, astrocytes, and neurons to generate the unique barrier properties of the blood–brain barrier (BBB), which is part of the

M. Dan • R. A. Yokel
Graduate Center for Toxicology, University of Kentucky
Lexington, Kentucky 40536, USA

T. A. Pittman
Department of Neurosurgery, University of Kentucky
Lexington, Kentucky 40536, USA

M. Dan
National Center for Safety Evaluation of Drugs, National Institutes for Food and Drug Control, Beijing 100176, China

M. Dan • Y. Bae • R. A. Yokel (✉)
Department of Pharmaceutical Sciences, College of Pharmacy, University of Kentucky Academic Medical Center, 335 Biopharmaceutical Complex (College of Pharmacy) Building, Lexington, Kentucky 40536-0596, USA
e-mail: ryokel@uky.edu

neurovascular unit that plays a crucial role in safeguarding the brain from potentially harmful endogenous and exogenous substances circulating in the blood. The BBB, with its tight junctions and efflux transporters, restricts the entry of most therapeutic agents, frequently resulting in unsuccessful treatment of brain diseases (1). Because of this challenge, research efforts have focused for decades on the development of strategies to more effectively deliver drugs to the central nervous system (CNS). A promising approach to overcome limited drug flux into the CNS is the employment of multifunctional nanoparticles (2). Numerous studies have shown that nanoparticle uptake into brain parenchyma can occur through receptor-mediated endocytosis, absorptive transcytosis, and tight junction opening (3,4). However, many *in vivo* reports of nanoparticle CNS applications, particularly those of metal-based nanoparticles, showed only indirect evidence of flux across the BBB into brain parenchyma. Given the distance between microvessels in the brain is less than 20 μm (e.g. see (5)), to be able to definitively state that a nanomaterial has crossed the *in vivo* BBB requires a high resolution imaging method, such as electron microscopy or confocal laser scanning microscopy, or a separation method such as described by Triguero *et al.* (6). Many reports concluded the nanomaterial entered the brain based on elemental analysis, fluorescence, or radioactivity using detection methods that do not differentiate substances in the vascular compartment of the brain or associated with the BBB *vs.* brain parenchyma, such as elemental analysis, e.g. (7), radioactivity, e.g. (8), or based their conclusions only on therapeutic efficacy in an animal model (9). The ability of nanoparticles to distribute from the luminal to the basolateral sides of the BBB or blood-tumor barrier will determine whether they can deliver drugs to specific brain tissues, such as brain tumors. A better understanding of nanoparticle association/uptake with, and flux across, biological barriers including the highly regulated BBB, is urgently needed.

Superparamagnetic iron oxide nanoparticles (IONPs) are useful to provide insights into these issues as well as having diagnostic and therapeutic applications. They can be activated by an alternating magnetic field (AMF) to generate local hyperthermia (10). Iron oxide nanoparticles are known to generate heat due to molecular vibration under AMF. The mechanisms underlying the production of heat for nanoparticles of the size utilized in this study (<50 nm) include the Neel mode (rotation of the magnetic moment of the IONPs away from its crystal lattice toward the alternating magnetic field to minimize its potential energy, providing internal friction due to the movement of the magnetic moment) and rotational friction provided by the viscous drag of the suspending medium as the IONPs align with the magnetic field. Mild hyperthermia (40 to 44°C) is cytotoxic to tumor cells (11). AMF activation of IONPs leads to a localized hyperthermia resulting in brain cancer cell death *in vitro* and *in vivo* (12,13). Mild whole body hyperthermia can increase BBB permeability, which has potential for brain therapeutic application (14). Whole body hyperthermia (42°C for 0.5 h) significantly increased flux of doxorubicin delivered in a temperature-sensitive liposome across the BBB *in vitro* and *in vivo* (15). However, whole body hyperthermia led to heat stress and caused CNS toxicity, including edema (14,16). One possibility is to develop an IONP nanocarrier system which can generate local hyperthermia to increase BBB permeability and brain accumulation for potential CNS diagnostic and therapeutic applications. Whether the BBB permeability of IONPs can be enhanced by taking advantage of their unique superparamagnetic properties, such as AMF-induced hyperthermia, needs to be investigated.

There are few reports of IONP association/uptake with, and flux across, the BBB. A recent study evaluated the uptake transport of surface-modified IONPs by human-derived endothelial cells; no IONP flux across the cells was observed (17). The lack of IONP flux across the BBB limits their applications to target the brain for diagnostic and therapeutic applications.

In this study, conventional citrate-coated IONPs (citrate-IONPs) and cross-linked nanoassemblies loaded with IONPs (CNA-IONPs) (10) were used as IONP nanocarrier models to investigate the effect of AMF-induced hyperthermia on IONP permeability and flux across the BBB.

Citrate-IONPs were prepared by co-precipitating ferric and ferrous ions in the presence of ammonium hydroxide with citric acid as a stabilizer, while CNA-IONPs were prepared by forming IONPs inside the core of poly(ethylene glycol)-poly(aspartate) block copolymer cross-linked nanoassemblies. Our previous research showed that CNA-IONPs are stable for 30 h in cell culture medium in the absence and presence of AMF (10). No cytotoxicity was seen in mouse brain endothelial-derived (bEnd.3) cells exposed to ≤10 mg/mL CNA-IONPs for 30 h (10). Incorporating IONPs in CNAs significantly improved particle stability and biocompatibility compared to citrate coating, providing a promising IONP formulation. Citrate-IONPs, as one of the most common and commercially available IONPs, were used as a control.

The objective of this study was to determine the potential effect and mechanism of AMF-induced hyperthermia on IONP association/uptake with, and flux across, BBB models. We evaluated citrate-IONP and CNA-IONP association/uptake, flux across, and effects using two *in vitro* BBB models (bEnd.3 and Madin-Darby canine kidney II (MDCKII) cells) in Transwells®. Although bEnd.3 cells form tighter junctions than some other BBB-derived cell lines, such as bEnd.5 cells and mouse brain endothelial cell 4 (18), the confluent bEnd.3 cell monolayer does not recapitulate the degree of tightness of *in vivo* BBB junctions, which is typical for BBB models composed of only BBB-derived endothelial cells (19). The bEnd.3 cell layer model better represents the clinically relevant blood-tumor barrier than the BBB. To study a better BBB model, we

also used MDCKII cells, a non-cerebral-derived cell line, because they express the components of the BBB tight junctions, are known to form tight junctions very well (20,21), and have been used as a surrogate *in vitro* BBB model (22). Results of this study provide a better understanding how AMF-induced hyperthermia influences IONP cell association/uptake and flux across the BBB, which will be beneficial for improving their CNS applications, such as brain tumor diagnosis and therapy.

MATERIALS AND METHODS

Materials

The chemicals used to prepare the citrate-coated IONPs (citrate-IONPs) and cross-linked nanoassemblies loaded with superparamagnetic iron oxide nanoparticles (CNA-IONPs) have been described (10). The immortalized mouse brain endothelial cell line bEnd.3 (American Type Culture Collection, Manassas, VA) and MDCKII cells (European Collection of Cell Cultures, Salisbury, UK) were used. Dulbecco's Modified Eagle Medium (DMEM) and minimum essential medium with Earle's salts (MEM) were obtained from Mediatech, Manassas, VA. Fetal bovine serum (FBS) was obtained from Atlanta Biologicals, Lawrenceville, GA. Penicillin and streptomycin were obtained from Invitrogen, Grand Island, NY. Transwell® filters were obtained from Corning Costar, Lowell, MA. Ferrozine and neocuproine were obtained from the Hach Company, Loveland, CO. Lucifer yellow was obtained from Sigma-Aldrich, St. Louis, MO. Bicinchoninic acid assay kits (BCA Protein Assay Kits) were obtained from Thermo Fisher Scientific, Waltham, MA. Twelve well plates were obtained from BD Falcon, San Jose, CA.

Preparation and Characterization of Citrate-IONPs and CNA-IONPs

Citrate-IONPs and CNA-IONPs were synthesized and characterized as described (10,23). Briefly, citrate-IONPs were prepared by adding ammonium hydroxide dropwise to a mixture of ferric chloride hexahydrate (Fe^{3+}) and ferrous chloride tetrahydrate (Fe^{2+}) dissolved in deionized water (Fe^{3+}:Fe^{2+} = 2:1) under a nitrogen atmosphere at 85°C and then stabilizing the IONPs with citric acid (2 equivalents). The citrate-IONPs were collected by a magnet and washed repeatedly using ethanol prior to overnight vacuum drying. CNA-IONPs were prepared by a similar method, replacing citric acid with cross-linked poly(ethylene glycol)-poly(aspartate) block copolymer nanoassemblies comprising 5 kDa PEG and 40 repeating units of aspartate that were chemically conjugated with 1,8-diaminooctane. In contrast to citrate-IONPs, CNA-IONPs dispersed in water stably, and were thus purified by filtration and dialysis prior to freeze drying. Both citrate-IONPs and CNA-IONPs were prepared in bulk, stored in powder forms at −20°C, and reconstituted in aqueous solutions (PBS or cell culture medium) immediately before use. Their particle size was measured each time by DLS. The stability of citrate-IONPs (0.05 mg/mL) and CNA-IONPs (2.5 mg/mL) in the cell culture media described below was monitored for 6 h after 0.5 h exposure to 37°C, 43°C, or AMF using dynamic light scattering (DLS) analysis (90Plus Nano-Particle size distribution analyzer, Brookhaven Instruments, Holtsville, NY).

Cell Lines and Culture Conditions

bEnd.3 and MDCKII cells were cultured in DMEM and MEM with 10 and 5% FBS, respectively, and 100 U/ml penicillin and 100 mg/ml streptomycin at 37°C in a humidified incubator with 5% CO_2. They were used from passages 5 through 10 and 45 through 60, respectively.

Transwell® Cultures

bEnd.3 and MDCKII cells were seeded on Transwell® filters (4.67 cm^2 for the 6-well polycarbonate plate, pore size 3.0 μm) at a density of 200,000 cells/cm^2, and grown to a monolayer (Fig. 1). bEnd.3 assays were performed 7 to 10 days after seeding (24), when transendothelial electrical resistance was >120 Ω·cm^2, measured using a RMA321-Millicell-ERS voltohmmeter (Millipore Corp, Billerica, MA). The apparent permeability coefficient (P_{app}) of LY at 37°C was $3.81 \pm 0.17 \times 10^{-6}$ cm/s (Table I), similar to a previous report (24). MDCKII assays were performed 4 days after seeding (25), when resistance was >170 Ω·cm^2.

Ferrozine Iron Assay

The iron content of the nanoparticle dispersions, cell culture media, nanoparticle-loaded cells, and control cells was determined using a ferrozine assay (26,27). Fifty μL of appropriately diluted sample was mixed with 50 μL of 1.4 mM HCl and 20 μL 2 M ascorbic acid and incubated at 70°C for 1 h. After cooling to room temperature, 30 μL of iron detection reagent (6.5 mM ferrozine, 6.5 mM neocuproine, 2.5 M ammonium acetate, and 1 M ascorbic acid in water) was added. After 30 min, the solution in each tube was transferred into a well of a 96 well plate and absorbance measured at 550 nm on a microplate reader. A standard curve was prepared with 0, 0.1, 0.2, 0.5, 1, 2, 5, and 10 μg/mL iron, and similarly treated.

AMF-Induced Heating Profiles

The heating profiles of AMF-activated CNA-IONPs (2.5 mg/mL) were evaluated in the Transwell® cell model. The heating

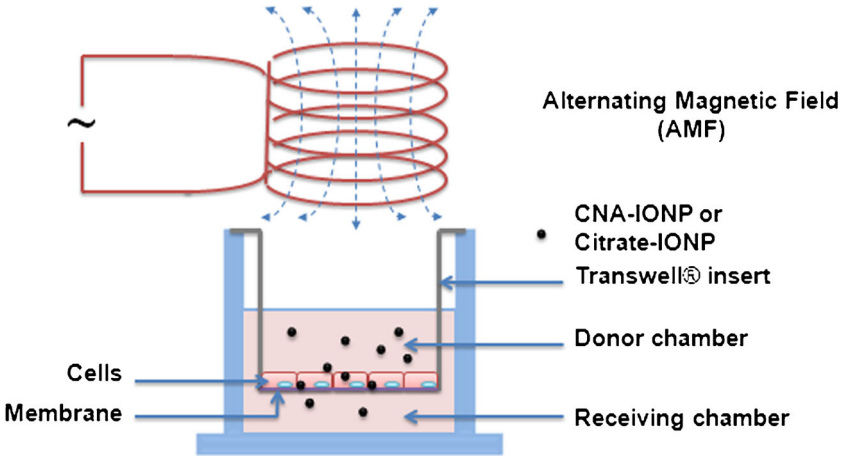

Fig. 1 Schema of the Transwell® system and AMF used for cell association/uptake and flux studies.

profile for citrate-IONPs was not studied because our previous study showed that 0.05 mg/mL IONPs provide insufficient iron to increase the cell culture medium temperature and higher concentrations kill the cells (10). AMF was induced by a Taylor Winfield induction power supply (Taylor-Winfield Technologies MMF-3-135/400-2, Columbus, OH) equipped with a 15 mm diameter, 5 turn solenoid. The AMF field parameters were 33.4 kA/m at 300 kHz. The temperature of the medium in the Transwell® donor chamber was measured every 0.25 s using a Fluoroptic® thermometer (LumaSense Technologies, Santa Clara, CA). The initial medium temperature was 37°C.

Paracellular Flux

To measure paracellular pathway permeability, 100 μM LY was added to the Transwell® donor side medium in every flux study. Media samples (100 μL) from the donor chamber were collected at time zero and from the receiving chamber at different times for LY quantification. LY concentration was measured in the donor and receiving chamber at the end of each experiment. Fluorescence was determined in a SpectraMax M5 Multi-Mode Microplate Reader (Molecular Devices, Sunnyvale, CA) at $\lambda_{ex}/\lambda_{em}$ = 450/530 nm and compared with a standard curve with a linear range from 0.5 to 30 μM in DMEM (bEnd.3 cells) or MEM (MDCKII cells) (28).

Table I Lucifer Yellow and CNA-IONP Apparent Permeability Coefficients

Cell Type	Sample	37°C	43°C (0.5 h)	AMF (0.5 h)
bEnd.3	Lucifer yellow	3.81 ± 0.17	4.04 ± 0.14	7.25 ± 0.28 *
	CNA-IONPs	0.67 ± 0.09	0.67 ± 0.09	1.66 ± 0.37 *
MDCKII	Lucifer yellow	0.49 ± 0.03	0.49 ± 0.049	0.59 ± 0.04 *
	CNA-IONPs	0.057 ± 0.008	0.056 ± 0.011	0.13 ± 0.02 *

The table shows apical-to-basolateral P_{app} coefficients of LY and CNA-IONPs using bEnd.3 and MDCKII *in vitro* BBB models at 37°C for 6 h ($n = 3$), 43°C (0.5 h) followed by 37°C for 6 h ($n = 3$), or AMF (0.5 h) followed by 37°C for 6 h ($n = 4$). P_{app} values are shown as 10^{-6} cm/s

* Significantly different compared to 37 and 43°C ($P < 0.05$)

Citrate-IONP and CNA-IONP Cell Association/Uptake and Flux Using bEnd.3 and MDCKII *In Vitro* BBB Models

Citrate-IONPs (0.05 mg/mL) or CNA-IONPs (2.5 mg/mL) and 100 μM LY were introduced into the Transwell® donor chamber. The concentrations were based on results of our previous cytotoxicity study (10). To determine cell association/uptake the cells were exposed to 37 or 43°C (the latter to compare to AMF-induced hyperthermia) or AMF for 0.5 h. All were then maintained at 37°C for 6 h. IONP cell association/uptake was terminated by medium removal and addition of ice cold solution containing 137 mM NaCl and 10 mM HEPES at pH 7.4 (29). Cells were trypsinized using 0.25% trypsin-EDTA for 5 min at 37°C and the suspension centrifuged. The cell pellet was re-suspended with medium. A trypan blue exclusion test was performed to assess cell viability (30). Protein concentrations were measured using the BCA Protein Assay Kit. At least three replications of the cell association/uptake experiments were conducted. To determine CNA-IONP flux across the MDCKII *in vitro* BBB model, CNA-IONPs (2.5 mg/mL) and LY were added to the donor chamber medium. The cells were incubated for 0.5, 1, 2, or 4 h at 43°C or exposed to 0.5 h AMF-induced hyperthermia followed by incubation at 37°C for 6 h. These experiments were performed in triplicate wells and repeated once in triplicate wells.

Citrate-IONP and CNA-IONP Cell Localization Using Transmission Electron Microscopy

bEnd.3 and MDCKII cells were seeded on 12 well plates at a density of 200,000 cells/cm^2. A cell association/uptake experiment was performed 3 days after seeding. The cells were exposed to cell culture medium containing 0.05 mg/mL citrate-IONPs or CNA-IONPs for 2 h, and then quickly washed with ice cold saline 3 times. The cells were fixed in 3.5% glutaraldehyde in 0.1 M cacodylate buffer, pH 7.4 for 1 h at 4°C. Samples were dehydrated in ascending

concentrations of ethanol and embedded in Eponate 12. After polymerization, blocks were sectioned at 80 nm and viewed with a Philips Tecnai 12 Biotwin electron microscope (FEI, Hillsboro, OR).

Data and Statistical Analysis

The apparent permeability coefficient (P_{app}) of LY and CNA-IONPs and their influx rates were calculated by linear regression. The P_{app} (in cm/s) was calculated using the equation: $P_{app} = (\Delta Q/\Delta t)/(\text{area}*C_D)$ (25). $\Delta Q/\Delta t$ is the linear appearance rate obtained from the profile of the transported amount of the substrate against time (mg/s). Area is the surface area of the cell monolayer (4.67 cm^2 for a 6-well plate). C_D is the initial donor concentration of LY or nanoparticle (mg/mL). Results from the first 6 h of flux data were used when the linear regression R^2 was >0.8. The % of IONPs / LY in receiving chamber = mass amount of IONPs/LY in the receiving chamber at certain time point × 100%/ initial donor dose. Mass balance of LY = (LY in the receiving and donor chambers) × 100%/ initial donor dose. Bartlett's test was used to determine if samples had equal variances. One-way ANOVA followed by Tukey's test was used to test for significant differences between citrate-IONP and CNA-IONP cell association/uptake and apparent permeability coefficients among the treatment groups. Two-way ANOVA followed by the Bonferroni multiple comparisons procedure was used to identify significant flux differences among the treatment groups and times using GraphPad Prism. The results of the statistical analysis for one-way and two-way ANOVAs are reported as F(df effect, df error) = *F*-value and *P*-value. All statistical tests were conducted using GraphPad Prism (GraphPad Software, San Diego, CA). All results are reported as mean ± standard deviation (SD). Statistical significance was accepted at $p < 0.05$.

RESULTS

Characterization of Citrate-IONP and CNA-IONP Size, Stability, and AMF Response

Citrate-IONPs had a primary particle size of ~10 nm, were 90 ± 10 nm in water at 0.2 mg/mL, but agglomerated to >400 nm and precipitated in PBS and cell culture medium (10). This agglomeration was accelerated by conventional (43°C) and AMF-induced hyperthermia, resulting in >800 nm agglomerates (results not shown).

The CNA-IONPs were 25 ± 3 nm measured by DLS. IONP loading of CNAs was 25 ± 3 and 25 ± 1 wt % determined by thermogravimetric analysis and inductively coupled plasma mass spectrometry analysis, respectively. AMF-induced hyperthermia had no effect on CNA-IONP size in cell culture medium at 30 h (Fig. 2a). AMF activation of CNA-IONPs (2.5 mg/mL) in cell culture medium increased the medium temperature to 41°C in 10 min (Fig. 2b).

Citrate-IONP and CNA-IONP Association/Uptake and Flux Using a bEnd.3 *In Vitro* BBB Model

Citrate-IONP cell association/uptake significantly increased in the conventional hyperthermia and AMF-induced hyperthermia groups compared to control ($F(2,6) = 24$, $P < 0.0014$) (Fig. 3a). In contrast, analysis of iron concentration showed CNA-IONP cell association/uptake did not change significantly in the conventional hyperthermia or the AMF-induced hyperthermia groups compared to the 37°C controls (Fig. 3b). TEM observations provided insight into the different cell association/uptake iron levels. Agglomerated citrate-IONPs (close to micrometer size) (Fig. 4a) with their primary size around 10 nm (Fig. 4b) were observed inside bEnd.3 cells. After analysis of three separately prepared TEM samples and two sections from each sample, CNA-IONPs were occasionally found in three samples (Fig. 4c). CNA-IONP cell association was at least 10 times lower compared with citrate-IONPs (Fig. 3b *vs.* a; Fig. 4c *vs.* b).

Flux of citrate-IONPs through the bEnd.3 monolayer did not increase over 6 h and was similar among the three treatment groups (Fig. 3c). The flux of CNA-IONPs significantly increased from 1 to 6 h in the AMF-induced hyperthermia group compared with the control and conventional hyperthermia groups (Fig. 3d). The paracellular flux rates measured by LY were linear for the first 6 h in the presence of citrate-IONP- (Fig. 3e) and CNA-IONP- (Fig. 3f) treated groups. Mass balance of LY for the bEnd.3 model was between 89 and 112%. Paracellular flux of LY in the CNA-IONP treated group, but not the citrate-IONP-treated group, was significantly increased in the AMF-induced hyperthermia group from 2 to 6 h (Fig. 3e and f). The P_{app} of LY was similar in the control and conventional hyperthermia groups in the presence of citrate-IONPs and CNA-IONPs (Fig. 3e and f; Table I). However, the P_{app} of CNA-IONPs in the AMF-induced hyperthermia group significantly increased (148%; $F(2,7) = 19$, $P < 0.0016$), and LY to a lesser extent (90%; $F(2,7) = 280$, $P < 0.0001$), compared with the normothermic control group (Table I). The trypan blue exclusion test showed no cell death in any experiments (results not shown). Since the flux was linear only for the first 6 h, the rest of this study only observed the flux rate for 6 h.

Effect of AMF-Induced *vs.* Conventional Hyperthermia on CNA-IONP Cell Association/Uptake and Paracellular Flux Using a MDCKII *In Vitro* BBB Model

In the absence of AMF-induced hyperthermia, CNA-IONP and LY flux were temperature- and concentration-

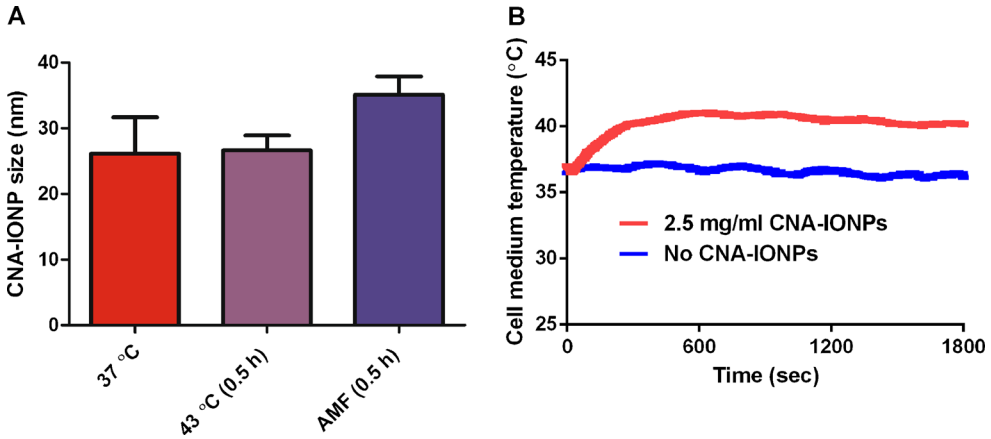

Fig. 2 AMF did not change CNA-IONP nanoparticle size but produced hyperthermia. Particle stability characterization results determined by DLS after exposure to 37°C for 30 h ($n = 6$), 43°C (0.5 h) followed by 37°C for 30 h ($n = 6$), or AMF (0.5 h), followed by 37°C for 30 h ($n = 4$) (**a**). Representative heating profile of CNA-IONPs in cell culture medium for fine-tuned remote heating with 0.5 h application of AMF (**b**). Cell culture medium exposed to AMF that contained no CNA-IONPs (37°C) served as the control.

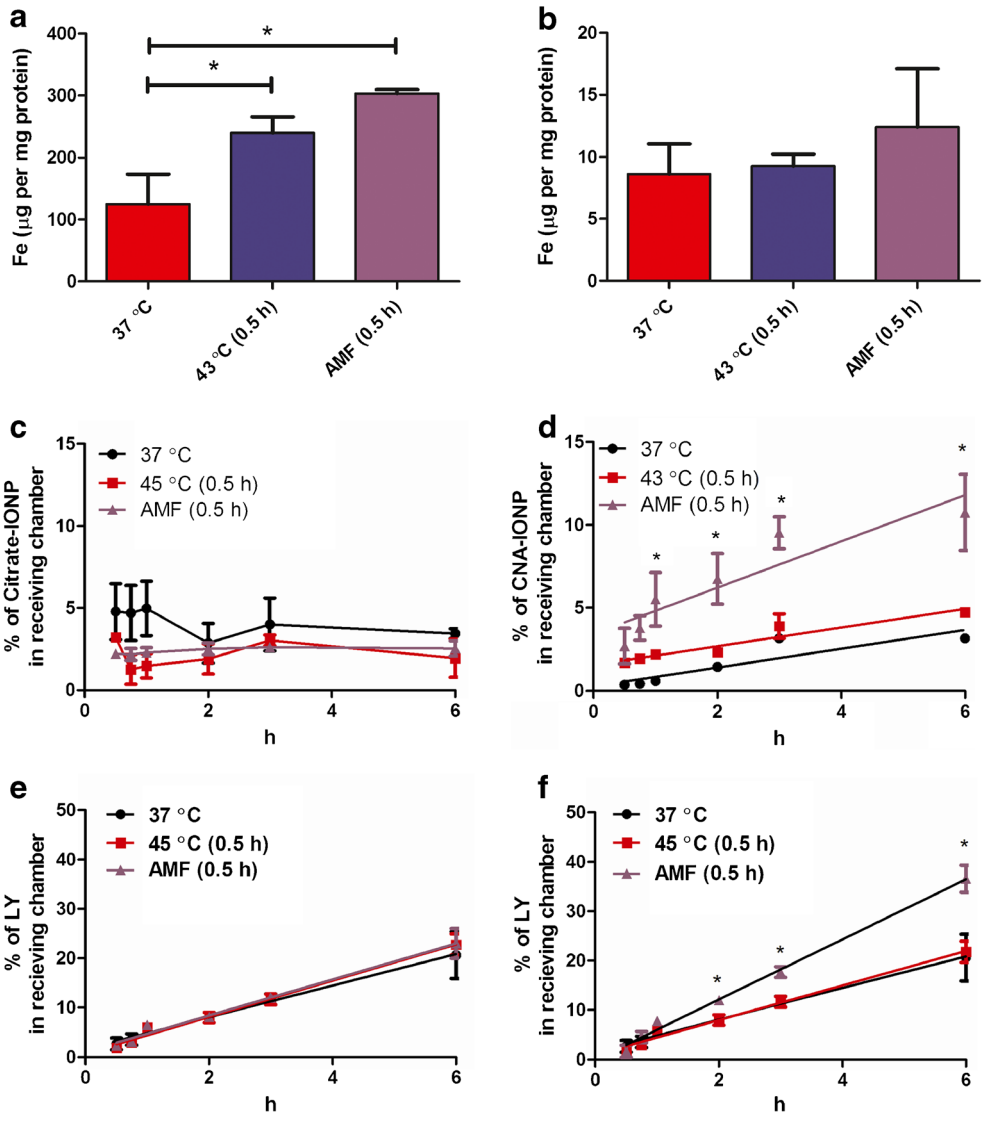

Fig. 3 Citrate-IONP and CNA-IONP cell association/uptake and flux across bEnd.3 cells. Citrate-IONP bEnd.3 cell association/uptake after 37°C for 6 h ($n = 3$), conventional hyperthermia at 43°C (0.5 h) followed by 37°C for 6 h ($n = 3$), or AMF-induced hyperthermia (0.5 h) followed by 37°C for 6 h ($n = 3$) (**a**). CNA-IONP bEnd.3 cell association/uptake after 37°C for 6 h ($n = 3$), conventional hyperthermia at 43°C (0.5 h) followed by 37°C for 6 h ($n = 3$), or AMF-induced hyperthermia (0.5 h) followed by 37°C for 6 h ($n = 4$) (**b**). Citrate-IONP flux across bEnd.3 cells (**c**). CNA-IONP flux across bEnd.3 cells (**d**). The paracellular flux across bEnd.3 cells measured by LY for the first 6 h in the Citrate-IONP treated group (**e**) and CNA-IONP treated group (**f**). Error bars not seen in panels C, D, E, and F are less than the symbol height. * Significantly different compared to 37°C in panel A or compared to 37°C and conventional hyperthermia in panel D and panel F.

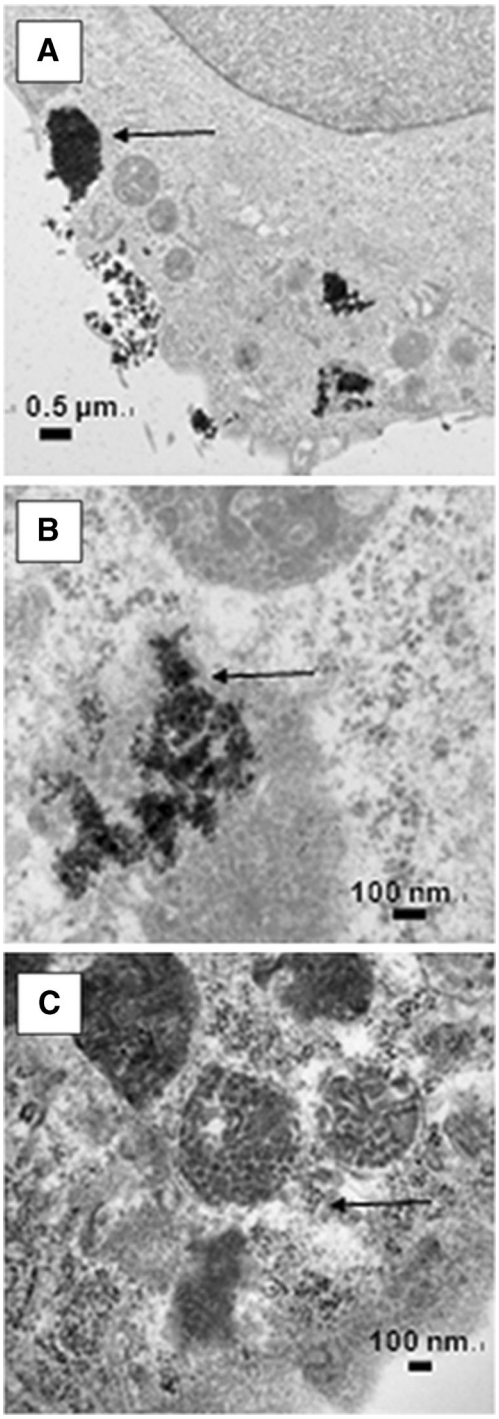

Fig. 4 Citrate IONP and CNA-IONP cell localization. Transmission electron microscopy results of the cellular localization of the Citrate-IONPs (**a** and **b**) and CNA-IONPs (**c**) in bEnd.3 cells at 2 h. The arrows indicate the location of IONPs inside the cells.

independent in the MDCKII *in vitro* BBB model (Fig. 5). Total flux was <0.2% over 6 h. MDCKII cell association/uptake of CNA-IONPs was significantly increased in the AMF-induced hyperthermia group compared to the control and conventional hyperthermia groups ($F(2,7) = 10$, $P<0.0081$) (Fig. 6a). AMF-induced hyperthermia significantly increased CNA-IONP flux (Fig. 6b). The P_{app} of CNA-IONPs ($F(2,7) = 27$, $P<0.0005$) increased much more than LY ($F(2,7) = 7$, $P<0.019$) in the AMF group, 128% and 20%, respectively, compared with controls (Table I). The trypan blue exclusion test showed no cell death in any experiments (results not shown). Lucifer yellow P_{app} was $0.49\pm0.03\times10^{-6}$ cm/s at 37°C (Table I). The LY P_{app} was 0.46 to 0.50×10^{-6} cm/s for the first 6 h after 0.5, 1, and 2 h exposure at 43°C followed by 37°C for 6 h. However, after incubation at 43°C for 4 h, the P_{app} of LY significantly increased 22% (P_{app}, $0.61\pm0.05\times10^{-6}$ cm/s) compared with the normothermic control and similar to the LY P_{app} across MDCKII cells 6 h after exposure to AMF-induced hyperthermia for 0.5 h (Table I). Paracellular flux (LY) was significantly greater across the MDCKII cells starting 2 h after exposure to AMF-induced hyperthermia (0.5 h) compared with the control and conventional hyperthermia (Fig. 6c). Mass balance of LY for the MDCKII model was between 92 and 108%. The trypan blue exclusion test did not reveal cell death in any experiments after cell exposure to 43°C for 4 h, or AMF-induced hyperthermia for 0.5 h, followed by 6 h at 37°C (results not shown).

DISCUSSION

Biocompatibility and stability in biological environments, such as cell culture medium or blood, are crucial for nanoparticles to serve as good candidate carriers across the BBB (31,32). In this study, we investigated citrate-IONP and CNA-IONP association/uptake, flux across, and effects on two *in vitro* models of the BBB under normothermic, conventional hyperthermic, and AMF-induced hyperthermic conditions. Citrate-IONPs agglomerated very rapidly in cell culture medium to >400 nm (10). Increased temperature enhanced their agglomeration. Even though citrate-IONPs agglomerated close to micrometer size *in vitro*, they were still able to be taken up by BBB cells. The TEM results suggested that citrate-IONPs were taken up by endocytosis. Citrate-IONPs did not show increased flux across bEnd.3 cells over 6 h, nor did increased temperature induced by conventional hyperthermia or AMF increase citrate IONP flux across bEnd.3 cells. Our results demonstrated that citrate-IONPs can enter BBB cells through an endocytosis pathway, however, they did not cross the *in vitro* BBB model. No transcytosis of citrate-IONPs across the BBB suggests they lack potential therapeutic CNS applications.

CNA incorporation of IONPs improved its stability (size ~25 nm, Fig. 2a) and biocompatibility compared to citrate IONPs, without loss of AMF-induced hyperthermia properties (10). Our previous research demonstrated that CNAs prepared from biocompatible poly(ethylene glycol)-poly(aspartate) [PEG-p(Asp)] block copolymers provided stability for nanoparticles, by entrapping them in the core of a

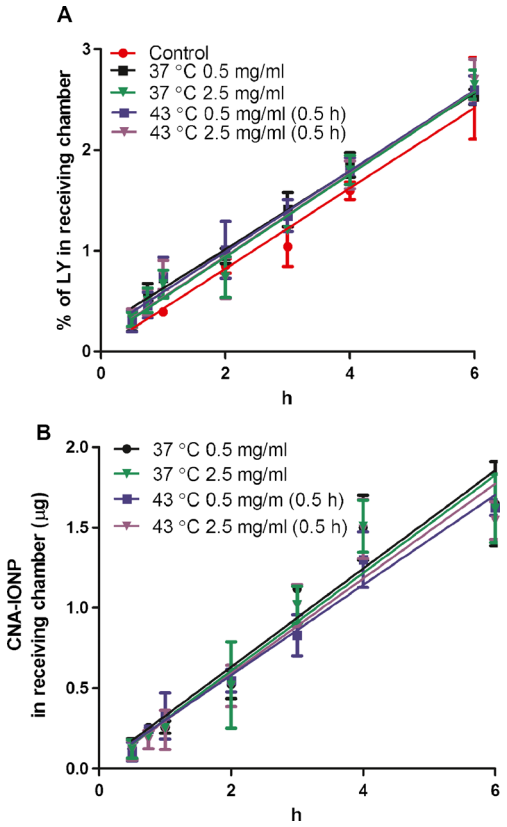

Fig. 5 Paracellular permeability and CNA-IONP flux across the MDCKII *in vitro* BBB model. LY (**a**) and CNA-IONP (**b**) flux at 2 concentrations and 2 temperatures ($n = 3$).

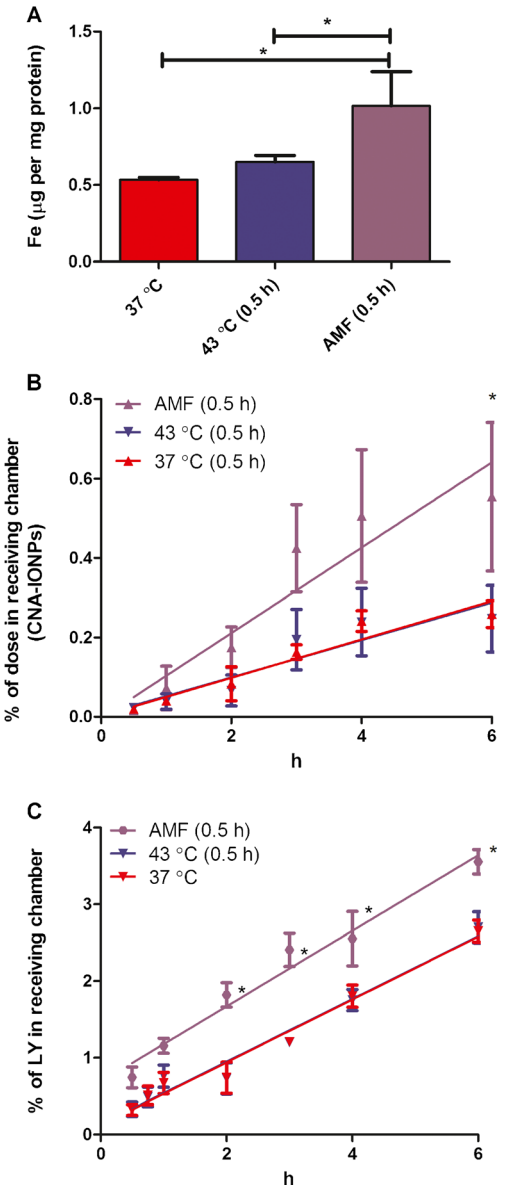

Fig. 6 CNA-IONP cell association/uptake and CNA-IONP and Lucifer yellow flux across MDCKII cells. CNA-IONP MDCKII cell association/uptake after 37°C for 6 h ($n = 3$), conventional hyperthermia at 43°C (0.5 h) followed by 37°C for 6 h ($n = 3$), or AMF-induced hyperthermia (0.5 h) followed by 37°C for 6 h ($n = 4$) (**a**). CNA-IONP flux across a MDCKII *in vitro* BBB model (**b**). The effect of conventional and AMF-induced hyperthermia on LY flux across MDCKII cells after 43°C incubation ($n = 3$) or AMF for 0.5 h followed by 37°C for 6 h ($n = 4$), compared to 37°C control ($n = 3$) (**c**). * Significantly different compared to AMF (0.5 h) in panel A or compared to 37°C and conventional hyperthermia in panels B and C.

charged cage produced by locally highly concentrated carboxylate groups that isolate the CNAs and stabilize them from interaction among themselves and environmental cations. CNAs provide the ability to incorporate hydrophobic and amphiphilic payloads without changing particle size (23,33). CNA-IONP flux increased with time across bEnd.3 cells at 37°C, resulting in flux of less than 5% in 6 h. Flux across MDCKII cells was less than 0.2%. We also demonstrated that CNA-IONP flux was concentration independent, providing evidence that it was through a non-diffusion mechanism (Fick's law). More studies are needed to investigate the mechanisms of IONP flux across the BBB. This very limited IONP flux is consistent with a report of charged IONP flux using a human brain derived BBB model, in which they did not observe any IONP flux over 24 h (17). The P_{app} (0.05 to 1×10^{-8} cm/s) of eleven iron oxide 200 to 1100 nm particles investigated using a bEnd.3 BBB model marginally supported the conclusion that larger particles have increased difficulty crossing the BBB (34). The P_{app} of CNA-IONPs is at least 10 times higher than these results. CNA-IONPs, with a relatively stable size <40 nm in cell culture medium, showed their greater ability to cross the BBB than other IONP carriers.

AMF-induced hyperthermia doubled the P_{app} of CNA-IONPs in the bEnd.3 model during the first 6 h. Ten percent of CNA-IONPs crossed the bEnd.3 monolayer within 6 h. The LY flux was also significantly increased, providing evidence that AMF-induced hyperthermia in the presence of CNA-IONPs opened the paracellular pathway to increase CNA-IONP flux. The lack of observed cell death ruled that out as the cause of increased flux. The cell uptake/association of CNA-IONPs was ~10 times lower than citrate-IONPs. The

low cell uptake of CNA-IONP was consistent with CNA-IONPs crossing the BBB mainly through the paracellular pathway after AMF-induced hyperthermia in the bEnd.3 *in vitro* BBB model. A recently published study also demonstrated that a static externally-applied magnetic field can increase IONP permeability through the paracellular pathway of bEnd.3 cells *in vitro* (35). The present report is the first to show that AMF-induced hyperthermia significantly increases CNA-IONP flux across in an *in vitro* BBB model with low toxicity. AMF-induced hyperthermia mediated by IONPs is one approach to potentially increase IONP BBB permeability and flux for CNS diagnosis and therapy.

The P_{app} of LY across MDCKII cells exposed to AMF increased only 20% compared to controls, whereas flux increased 90% in the bEnd.3 model. AMF-induced hyperthermia increased the P_{app} of CNA-IONPs 148% in the bEnd.3 model and 128% in the MDCKII model. In general, a similar trend was observed in BBB permeability changes (LY flux) induced by AMF-induced hyperthermia using the two *in vitro* BBB models. However, the 'leaky' bEnd.3 Transwell® model's paracellular pathway flux was more sensitive to conventional and AMF-induced hyperthermia than MDCKII cells. Previous studies also showed a threshold at 43°C for BBB disruption induced by conventional hyperthermia in normal brain tissue (36,37). However, in a leaky BBB, such as the blood-tumor barrier which was more sensitive to conventional hyperthermia, permeability increased at a lower temperature (38). The bEnd.3 Transwell® model can provide insight into the effect of AMF-induced hyperthermia on leaky BBB conditions such as the blood-tumor barrier. Even though MDCKII cells are not a BBB-derived cell line, they were shown to be a good *in vitro* model to predict the extent of brain exposure and the rate of brain association/uptake *in vivo* for several CNS drug candidates (39). However, there are major differences between MDCKII epithelial and brain endothelial cells, such as expression of different transporters (40). Comparing these two *in vitro* BBB models, the MDCKII cell model better predicts whether AMF-induced hyperthermia changes paracellular flux in normal brain tissue because they form tighter junctions than the bEnd.3 cells. Because of the unique physicochemical properties and different cell association/uptake mechanisms of nanoparticles compared with small drug candidates, further studies were needed to investigate the correlation between nanoparticle flux across the bEnd.3 and MDCKII Transwell® models and the BBB *in vivo*.

The potential application of conventional hyperthermia to increase BBB permeability has been investigated for decades. Numerous studies showed that conventional hyperthermia can increase BBB permeability depending on heat magnitude and duration (14,16). However, the difference between conventional hyperthermia and AMF-induced hyperthermia on BBB permeability has not been well studied. The P_{app} of LY and CNA-IONPs significantly increased (90 and 148% respectively) in the AMF-induced hyperthermia group compared with the conventional hyperthermia group bEnd.3 cells. There was no significant difference between the 37 and 43°C groups, suggesting AMF-activation of CNA-IONPs increased BBB permeability not only by simple heating but also other factors such as IONP vibration or difference in IONP surface temperature *vs.* the surrounding temperature. CNA-IONPs can bind to the cell surface and vibrate under AMF, mechanically increasing BBB permeability. Other research demonstrated that cell surface bound IONPs can mechanically activate certain cell surface receptors (41). The temperature we measured was the environmental temperature in the Transwell® medium rather than the IONP surface temperature. Previous research showed that IONP surface temperature can be up to 20°C higher relative to the surrounding regions (42). Further research needs to be conducted to investigate how CNA-IONPs associate with BBB cells and the role of temperature and mechanical effects on BBB permeability.

AMF-induced hyperthermia can increase paracellular permeability more effectively than conventional hyperthermia. Our results showed that conventional hyperthermia (43°C) did not influence paracellular flux up to 2 h and that flux significantly increased at 43°C after 4 h. A previous whole body hyperthermia study with rats also showed BBB permeability changes were highly dependent on heat magnitude and duration. No BBB permeability change was observed (within 2 h) under whole body hyperthermia, but BBB permeability increased after 4 h whole body hyperthermia (16). We did not observe any cell death even after 4 h conventional hyperthermia at 43°C. However, whole body hyperthermia leads to heat stress causing numerous CNS toxicities such as edema and neuropil damage (43). Our results also showed that the P_{app} of LY after conventional hyperthermia at 43°C for 4 h was similar to the P_{app} of LY at AMF-induced hyperthermia for 0.5 h. AMF-induced hyperthermia can increase BBB permeability similar to conventional hyperthermia at a lower cell medium temperature and shorter time without cell death *in vitro*. Previous research showed that 0.5 h AMF-induced hyperthermia killed head and neck cancer cells in mice without harming normal cells (44). Furthermore, previous research also demonstrated that AMF-induced hyperthermia only led to a transient BBB permeability increase *in vivo*. Their results showed that 0.5 h AMF-induced hyperthermia can increase the BBB permeability transiently and the BBB permeability recovered 2 h after hyperthermia treatment in mice (45). In the present study AMF-induced hyperthermia showed the potential advantages of transiently increased BBB permeability and reduced toxicity compared with conventional hyperthermia, potentially increasing the brain targeting of IONPs and their pharmacotherapeutic efficacy.

CONCLUSIONS

CNA-IONPs showed stability in a mammalian tissue (cell culture) relevant medium. Flux across bEnd.3 and MDCKII *in vitro* BBB models was low under normothermic conditions. AMF-induced hyperthermia for 0.5 h enhanced CNA-IONP cell association/uptake and flux in the absence of cell death. In contrast, citrate IONPs agglomerated in cell culture medium and were taken up by, but did not flux through, the bEnd.3 BBB model. AMF-induced hyperthermia enhanced the BBB association/uptake and permeability of CNA-IONPs more effectively than conventional hyperthermia, by mechanisms in addition to elevated temperature around the IONPs. CNA-IONPs activated by AMF can produce a quantifiable, controllable hyperthermia in a defined area which is required for clinical applications. AMF-induced hyperthermia provides an approach to deliver IONPs across the BBB with low toxicity for potential therapeutic and diagnostic CNS applications.

ACKNOWLEDGMENTS AND DISCLOSURES

The authors gratefully acknowledge J. Zack Hilt for sharing his AMF equipment and the citrate-IONP synthesis method, Daniel F. Scott for assisting in CNA synthesis, and Markos Leggas and Kuei-Ling Kuo for providing the MDCKII cell line and assisting in the Transwell® model establishment. Mo Dan and the project described were supported by Grant Number R25CA153954 from the National Cancer Institute. The content is solely the responsibility of the authors and does not necessarily represent the official views of the National Cancer Institute or the National Institutes of Health.

REFERENCES

1. Bernacki J, Dobrowolska A, Nierwinska K, Malecki A. Physiology and pharmacological role of the blood–brain barrier. Pharmacol Rep. 2008;60(5):600–22.
2. Agarwal A, Lariya N, Saraogi G, Dubey N, Agrawal H, Agrawal GP. Nanoparticles as novel carrier for brain delivery: a review. Curr Pharm Des. 2009;15(8):917–25.
3. Peetla C, Labhasetwar V. Biophysical characterization of nanoparticle-endothelial model cell membrane interactions. Mol Pharm. 2008;5(3):418–29.
4. Dhanikula RS, Hammady T, Hildgen P. On the mechanism and dynamics of uptake and permeation of polyether-copolyester dendrimers across an *in vitro* blood–brain barrier model. J Pharm Sci. 2009;98(10):3748–60.
5. Boström M, Hellstroem Erkenstam N, Kaluza D, Jakobsson L, Kalm M, Blomgren K. The hippocampal neurovascular niche during normal development and after irradiation to the juvenile mouse brain. Int J Radiat Biol. 2014;90(9):778–89.
6. Triguero D, Buciak J, Pardridge WM. Capillary depletion method for quantification of blood–brain barrier transport of circulating peptides and plasma proteins. J Neurochem. 1990;54(6):1882–8.
7. Zhang L, Bai R, Li B, Ge C, Du J, Liu Y, *et al.* Rutile TiO_2 particles exert size and surface coating dependent retention and lesions on the murine brain. Toxicol Lett. 2011;207(1):73–81.
8. Wang J, Chen C, Liu Y, Jiao F, Li W, Lao F, *et al.* Potential neurological lesion after nasal instillation of TiO_2 nanoparticles in the anatase and rutile crystal phases. Toxicol Lett. 2008;183(1–3):72–80.
9. Ambruosi A, Gelperina S, Khalansky A, Tanski S, Theisen A, Kreuter J. Influence of surfactants, polymer and doxorubicin loading on the anti-tumour effect of poly(butyl cyanoacrylate) nanoparticles in a rat glioma model. J Microencapsul. 2006;23(5):582–92.
10. Dan M, Scott DF, Hardy PA, Wydra RJ, Hilt JZ, Yokel RA, *et al.* Block copolymer cross-linked nanoassemblies improve particle stability and biocompatibility of superparamagnetic iron oxide nanoparticles. Pharm Res. 2013;30(3):552–61.
11. van der Zee J. Heating the patient: a promising approach? Ann Oncol. 2002;13(8):1173–84.
12. Meenach SA, Anderson KW, Hilt JZ. Synthesis and characterization of thermoresponsive poly(ethylene glycol)-based hydrogels and their magnetic nanocomposites. J Polym Sci Part A: Polym Chem. 2010;48(15):3229–35.
13. Silva AC, Oliveira TR, Mamani JB, Malheiros SMF, Malavolta L, Pavon LF, *et al.* Application of hyperthermia induced by superparamagnetic iron oxide nanoparticles in glioma treatment. Int J Nanomed. 2011;6:591–603.
14. Kiyatkin EA, Sharma HS. Permeability of the blood–brain barrier depends on brain temperature. Neuroscience (Amsterdam, Neth). 2009;161(3):926–39.
15. Gong W, Wang Z, Liu N, Lin W, Wang X, Xu D, *et al.* Improving efficiency of adriamycin crossing blood brain barrier by combination of thermosensitive liposomes and hyperthermia. Biol Pharm Bull. 2011;34(7):1058–64.
16. Sharma HS, Hoopes PJ. Hyperthermia induced pathophysiology of the central nervous system. Int J Hyperthermia. 2003;19(3):325–54.
17. Kenzaoui BH, Bernasconi CC, Hofmann H, Juillerat-Jeanneret L. Evaluation of uptake and transport of ultrasmall superparamagnetic iron oxide nanoparticles by human brain-derived endothelial cells. Nanomedicine (Lond). 2012;7(1):39–53.
18. Watanabe T, Dohgu S, Takata F, Nishioku T, Nakashima A, Futagami K, *et al.* Paracellular barrier and tight junction protein expression in the immortalized brain endothelial cell lines bEND.3, bEND.5 and mouse brain endothelial cell 4. Biol Pharm Bull. 2013;36(3):492–5.
19. Abbott NJ, Dolman DEM, Drndarski S, Fredriksson SM. An improved in vitro blood–brain barrier model: rat brain endothelial cells co-cultured with astrocytes. Methods Mol Biol (N Y, NY, U S). 2012;814(Astrocytes: Methods & Protocols):415–30.
20. Kadam RS, Scheinman RI, Kompella UB. Pigmented-MDCK (P-MDCK) cell line with tunable melanin expression: an in vitro model for the outer blood-retinal barrier. Mol Pharm. 2012;9(11):3228–35.
21. Fazlollahi F, Angelow S, Yacobi NR, Marchelletta R, Yu ASL, Hamm-Alvarez SF, *et al.* Polystyrene nanoparticle trafficking across MDCK-II. Nanomedicine (Philadelphia, PA, U S). 2011;7(5):588–94.
22. Hellinger E, Veszelka S, Toth AE, Walter F, Kittel A, Bakk ML, *et al.* Comparison of brain capillary endothelial cell-based and epithelial (MDCK-MDR1, Caco-2, and VB-Caco-2) cell-based surrogate blood–brain barrier penetration models. Eur J Pharm Biopharm. 2012;82(2):340–51.
23. Lee HJ, Bae Y. Cross-linked nanoassemblies from poly(ethylene glycol)-poly(aspartate) block copolymers as stable supramolecular templates for particulate drug delivery. Biomacromolecules. 2011;12(7):2686–96.
24. Brown RC, Morris AP, O'Neil RG. Tight junction protein expression and barrier properties of immortalized mouse brain microvessel endothelial cells. Brain Res. 2007;1130(1):17–30.

25. Nozinic D, Milic A, Mikac L, Ralic J, Padovan J, Antolovic R. Assessment of macrolide transport using PAMPA, Caco-2 and MDCKII-hMDR1 assays. Croat Chem Acta. 2010;83(3):323–31.
26. Basel MT, Balivada S, Wang H, Shrestha TB, Seo GM, Pyle M, *et al.* Cell-delivered magnetic nanoparticles caused hyperthermia-mediated increased survival in a murine pancreatic cancer model. Int J Nanomed. 2012;7:297–306.
27. Riemer J, Hoepken HH, Czerwinska H, Robinson SR, Dringen R. Colorimetric ferrozine-based assay for the quantitation of iron in cultured cells. Anal Biochem. 2004;331(2):370–5.
28. Zhou Y, Harris WR, Yokel RA. The influence of citrate, maltolate and fluoride on the gastrointestinal absorption of aluminum at a drinking water-relevant concentration: A ^{26}Al and ^{14}C study. J Inorg Biochem. 2008;102:798–808.
29. Zhou Y, Yokel RA. The chemical species of aluminum influences its paracellular flux across and uptake into Caco-2 cells, a model of gastrointestinal absorption. Toxicol Sci. 2005;87(1):15–26.
30. Strober W. Trypan blue exclusion test of cell viability. In: Coligan JE, editor. Curr Protoc Immunol. 2001; Appendix 3B.
31. Bhaskar S, Tian F, Stoeger T, Kreyling W, de la Fuente JM, Grazu V, Borm P, Estrada G, Ntziachristos V, Razansky D. Multifunctional nanocarriers for diagnostics, drug delivery and targeted treatment across blood–brain barrier: perspectives on tracking and neuroimaging. Part Fibre Toxicol. 2010;7.
32. Neuberger T, Schoepf B, Hofmann H, Hofmann M, Von Rechenberg B. Superparamagnetic nanoparticles for biomedical applications: possibilities and limitations of a new drug delivery system. J Magn Magn Mater. 2005;293(1):483–96.
33. Scott D, Rohr J, Bae Y. Nanoparticulate formulations of mithramycin analogs for enhanced cytotoxicity. Int J Nanomed. 2011;6:2757–67.
34. Hoff D, Sheikh L, Bhattacharya S, Nayar S, Webster TJ. Comparison study of ferrofluid and powder iron oxide nanoparticle permeability across the blood–brain barrier. Int J Nanomed. 2012;8:703–10.
35. Sun Z, Worden M, Wroczynskyj Y, Yathindranath V, van Lierop J, Hegmann T, *et al.* Magnetic field enhanced convective diffusion of iron oxide nanoparticles in an osmotically disrupted cell culture model of the blood–brain barrier. Int J Nanomed. 2014;9:3013–26.
36. Moriyama E, Salcman M, Broadwell RD. Blood–brain barrier alteration after microwave-induced hyperthermia is purely a thermal effect: I. Temperature and power measurements. Surg Neurol. 1991;35(3):177–82.
37. Nakagawa M, Matsumoto K, Higashi H, Furuta T, Ohmoto T. Acute effects of interstitial hyperthermia on normal monkey brain–magnetic resonance imaging appearance and effects on blood–brain barrier. Neurol Med Chir (Tokyo). 1994;34(10):668–75.
38. Uzuka T, Takahashi H, Tanaka R. Interstitial hyperthermia with intra-arterial injection of adriamycin for malignant glioma. Neurol Med Chir (Tokyo). 2006;46(1):19–23. discussion 23.
39. Wang Q, Rager JD, Weinstein K, Kardos PS, Dobson GL, Li J, *et al.* Evaluation of the MDR-MDCK cell line as a permeability screen for the blood–brain barrier. Int J Pharm. 2005;288(2):349–59.
40. Wilhelm I, Fazakas C, Krizbai IA. In vitro models of the blood–brain barrier. Acta Neurobiol Exp (Wars). 2011;71(1):113–28.
41. Mannix RJ, Kumar S, Cassiola F, Montoya-Zavala M, Feinstein E, Prentiss M, *et al.* Nanomagnetic actuation of receptor-mediated signal transduction. Nat Nanotechnol. 2008;3(1):36–40.
42. Huang H, Delikanli S, Zeng H, Ferkey DM, Pralle A. Remote control of ion channels and neurons through magnetic-field heating of nanoparticles. Nat Nanotechnol. 2010;5(8):602–6.
43. Sharma HS, Sharma A, Moessler H, Muresanu DF. Neuroprotective effects of cerebrolysin, a combination of different active fragments of neurotrophic factors and peptides on the whole body hyperthermia-induced neurotoxicity: modulatory roles of co-morbidity factors and nanoparticle intoxication. Int Rev Neurobiol. 2012;102(New Perspectives of Central Nervous System Injury and Neuroprotection):249–76.
44. Sharma HS, Sharma A. Nanowired drug delivery for neuroprotection in central nervous system injuries: modulation by environmental temperature, intoxication of nanoparticles, and comorbidity factors. Wiley Interdiscip Rev Nanomed Nanobiotechnol. 2012;4(2):184–203.
45. Tabatabaei SN, Duchemin S, Girouard H, Martel S. Towards MR-navigable nanorobotic carriers for drug delivery into the brain. IEEE Int Conf Robot Autom. 2012;14:727–32.